J Mol Model (2011) 17:2717–2723
DOI 10.1007/s00894-010-0938-7

SHORT COMMENT

In silico study of the inhibition of DNA polymerase by a novel catalpol derivative

Osvaldo A. Martin · Hugo A. Garro · Marcela B. Kurina Sanz · Carlos Rodolfo Pungitore · Carlos E. Tonn

Received: 8 July 2010 / Accepted: 16 December 2010 / Published online: 13 January 2011

Abstract In this work, a novel catalpol derivative (6,10,2′,6′-tetraacetyl-*O*-catalpol), which was previously obtained by our group and shown experimentally to inhibit a type of *Taq* DNA polymerase, was studied in silico. Studies of the interaction of 6,10,2′,6′-tetraacetyl-*O*-catalpol with the Klentaq fragment of the *Taq* DNA polymerase I from *Thermus aquaticus* helped to elucidate the mechanism of inhibition of the enzyme, and offered valuable information that can be used to propose substrate structural modifications aimed at increasing the binding affinity. Classical and semi-empirical methods were used to characterize the conformational preferences of this organic compound in solution. Using docking simulations, the most probable binding mode was found, and the stabilities of the docked solutions were tested in a series of molecular dynamics experiments. Results indicated that the mechanism of inhibition may be competitive, which agrees with previous binding experiments done with 6,10,2′,6′-tetraacetyl-*O*-catalpol.

Keywords *Taq* DNA polymerase · Iridoid · Catalpol · Docking · Molecular dynamics

O. A. Martin
IMASL-CONICET, Universidad Nacional de San Luis. Ejército, de los Andes 950,
5700, San Luis, Argentina

H. A. Garro · M. B. Kurina Sanz · C. R. Pungitore (✉) · C. E. Tonn
INTEQUI-CONICET, Facultad de Química, Bioquímica y Farmacia, Universidad Nacional de San Luis,
Chacabuco y Pedernera,
5700, San Luis, Argentina
e-mail: crpungi@unsl.edu.ar

Introduction

Nature is an infinite resource for discovering new drugs and other bioactive compounds of interest. The plant kingdom represents a source of natural products, and only about 6% of these products have been studied for their biological activity, while about 15% of them have been studied by phytochemical methods [1].

Among these products, iridoids are group of irregular monoterpenes that are so named because of their structural and biosynthetic relationships with iridomyrmecin and iridodial compounds [2]. Biocatalysis has become a powerful tool for highly stereoselective and regioselective transformations, due to the intrinsic chirality of enzymes [3]. In particular, biocatalyzed regioselective transformations using hydrolases have been widely described in the literature [4]. They also constitute environmentally sensitive, milder and energy-saving methods that complement traditional chemical approaches to modifying natural products.

Catalpol is a glycosylated iridoid that shows biological activity against the enzyme DNA polymerase. It inhibits this enzyme with a IC_{50} value of 47.8 μM, according to a competitive inhibition mechanism [5]. DNA polymerases have recently emerged as important cellular targets for chemical intervention in the development of antitumor agents [6]. Atomic level three-dimensional structures of various types of polymerases and other enzymes related to nucleic acids, such as the Klenow fragment from DNA polymerase I of *Escherichia coli* and its counterpart Klentaq isolated from the bacterium *Thermus aquaticus*, are now available [6, 7].

In a previous work, 6,10,2′,6′-tetraacetyl-*O*-catalpol, a novel partially acetylated catalpol derivative, was prepared in our laboratory by the regioselective hydrolysis of

peracetylcatalpol mediated by whole-cell cultures of *Aspergillus niger* (Fig. 1). In the same work, we demonstrated that the new derivative was able to inhibit the enzyme *Taq* DNA polymerase with an IC_{50} value of 43.02 μM. It is thus reasonable to infer that the mechanism of action of 6,10,2′,6′-tetraacetyl-*O*-catalpol is probably competitive [8].

In order to confirm this hypothesis, as well as to design rational modifications of 6,10,2′,6′-tetraacetyl-*O*-catalpol that will increase its binding affinity, we tried to gain insight into the mode of binding of 6,10,2′,6′-tetraacetyl-*O*-catalpol to *Taq* DNA polymerase using computational methods.

Methods

File preparation

The Gabedit software package [9] was used to draw the 6,10,2′,6′-tetraacetyl-*O*-catalpol molecule. The geometry was initially optimized using the classic quasi-Newton method, followed by semiempirical optimization using the software MOPAC 2009 [10, 11], as implemented in Gabedit. This conformation was used to obtain the parameters and topology files for the GROMACS software package [12, 13] using the ProDGR server [14].

Conformational search

Two different approaches were used to determine the conformational space and identify the global minima of 6,10,2′,6′-tetraacetyl-*O*-catalpol.

Simulated annealing

The GROMACS 3.3 software package was used to perform a simulated annealing protocol. The forcefield used was ffG53a6, the solvent was explicitly simulated using the SPC model, periodic boundary conditions were implemented using the PME (particle mesh Ewald) algorithm [15], and the cut-off values were 1.4 nm and 0.9 nm for van der Waals and coulombic interactions, respectively. The pressure was kept constant at 1 atm. The temperatures of 6,10,2′,6′-tetraacetyl-*O*-catalpol and the solvent were controlled independently using two decoupled Berendsen thermostats.

Three runs were performed following different temperature variation schema: in the first run, the temperature of 6,10,2′,6′-tetraacetyl-*O*-catalpol was raised from 100 K to 1700 K in 75 ps, maintained at this for 25 ps, and then slowly lowered to 400 K in 1.1 ns. The temperature was decreased to 100 K in 200 ps and kept at 100 K for 100 ps. This procedure was repeated: setting the maximum temperature to 1000 K, both cycles were iterated until the total simulation time was 30 ns. Snapshots were saved every 1.5 ns (i.e., at the end of each heating–cooling cycle).

The second and third runs followed a similar but simplified scheme where the maximum temperatures were 2000 K and 1200 K, respectively. Snapshots were saved every 1.5 ns (i.e., at the end of each cycle).

The temperature of the solvent was independently controlled during each run. It was raised from 100 K to 400 K in 75 ps, maintained at this for 1.55 ns, and then slowly lowered to 100 K in 200 ps, where it was kept for 100 ps. It is important to note that during this last step both solute and solvent are at the same temperature, and they decrease in temperature simultaneously, as if their temperatures were controlled by only one thermostat. This decoupling–coupling temperature scheme allows the solute to reach a high temperature (and hence exceed the high energy barrier) while maintaining control over the kinetic energy of the solvent, and at the same time it also allows the solvation effect to be realistically modeled at low temperatures.

All of the resulting conformations were minimized with Gromacs, inspected visually, and ranked according to the energy value.

Molecular dynamics search

Yasara Dynamics 10 software [16] was used to perform a molecular dynamics search. A time step of 2 fs was used. The Amber03 forcefield [17] was selected; the simulation box allowed at least 10 Å around all of the atoms in 6,10,2′,6′-tetraacetyl-*O*-catalpol, and was filled with the TIP3 water model. Periodic boundary conditions were used

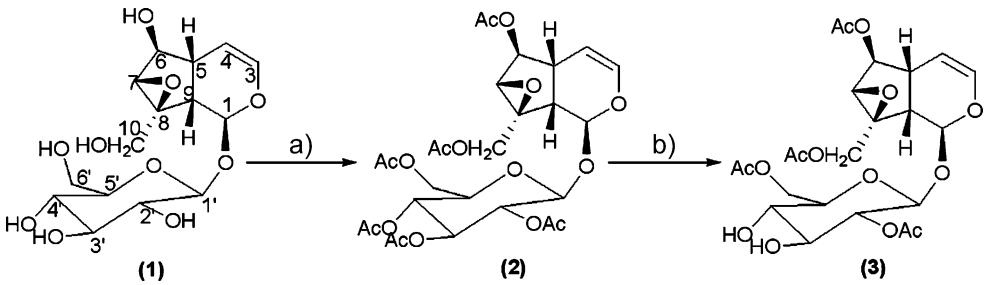

Fig. 1 Synthetic scheme for 6,10,2′,6′-tetraacetyl-*O*-catalpol, starting from catalpol. *a*) Ac_2O, dry piridine, t.a. 48 h; *b*) biotransformation using whole cells of *Aspergillus niger*

as implemented in the PME algorithm. Na^+ and Cl^- ions were added in order to properly simulate the ion strength in physiological solution. The temperature was fixed at 298 K and controlled by checking the velocities of the atoms every 25 simulation steps. The pressure was controlled by rescaling the box dimensions in order to maintain the water density at 0.997 g/l. Two simulations of 300 productive nanoseconds each were performed starting from (a) the best energy conformation identified during the simulated annealing procedure (where the torsion angles α=171.7° and β= 186.4°,;see the inset in Fig. 2) was minimized with the Amber03 force field, and (b) the same conformation as in (a), but with the torsion angle α rotated 180° and minimized with the Amber03 force field (Fig. 2). A snapshot taken every 25 ps was saved for further analysis. A conformational map representing the α (C2′-C1′-$O_{anomeric}$-C1) and β (C2′-C1′-$O_{anomeric}$-C9) torsion angles was built using QtiPlot 0.9.7 [18], and the torsion angles were binned every 2°. Geometry optimization of 6,10,2′,6′-tetracetil-*O*-catalpol was done in vacuo using MOPAC 2009 coupled to a shell script. The PM6 Hamiltonian and a termination criterion of gradient norm < 0.01 were used. Due to the computational cost of this task, the minimization was restricted to 600 conformations, i.e., one conformation per nanosecond.

Molecular docking

Autodock 4.0 [19, 20] was used to perform the molecular docking of 6,10,2′,6′-tetraacetyl-*O*-catalpol to the Klentaq fragment. The coordinates of the target molecule (including the Klentaq fragment and a short DNA portion) were taken from the Protein Data Bank [21] deposited under the accession code 2KTQ [22]. Two types of search were performed:

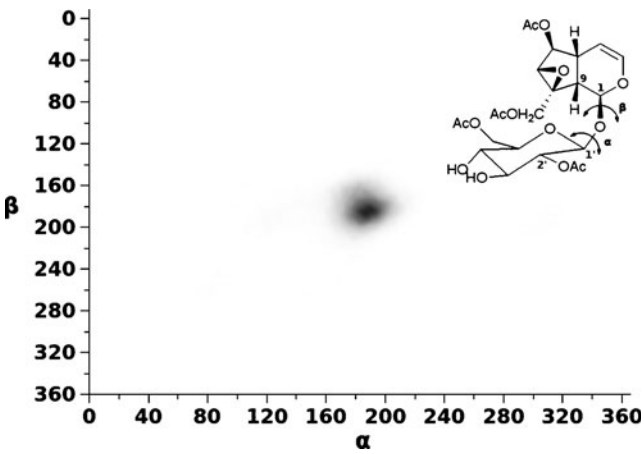

Fig. 2 Conformational map of the ad hoc defined torsion angles α and β, which fully determine the relative position of the terpenic fragment with respect to the glicosidic residue. *Inset*: α (C2′-C1′-$O_{anomeric}$-C1) and β (C2′-C1′-$O_{anomeric}$-C9) torsion angles are indicated with *double arrows*

- *Blind docking search*. This assumes no previous knowledge of the binding site. A grid spacing of 0.758 Å was used, ensuring that the whole target molecule was covered. The number of individuals was set at 250, the maximum number of evaluations was 3.5×10^6, and 200 runs were performed in total. These parameters were chosen following the recommendations of Hetényi et al. [23]. All other parameters took their default values. The flexibility of the ligand was considered fully.
- *Binding site restricted search*. A search restricted to the binding site was performed with the following parameters: population size of 150 individuals; maximum number of evaluations of 50×10^6; total number of 80 runs; and a grid spacing of 0.375 Å. The ligand was considered to be completely flexible. The binding site was defined as a box ~26 Å on a side that was centered near the position of the ddCTP in the original 2KTQ Protein Data Bank (PDB). This box was large enough to ensure the free rotation of the ligand.

Macromolecule–ligand molecular dynamics

Yasara Dynamics 10 was used to perform a classical molecular dynamics study of the two Klentaq/DNA/6,10,2′,6′-tetraacetyl-*O*-catalpol complexes obtained from the docking simulation, named solution A and solution B. Each complex was submitted to 30 ns of productive molecular dynamics. The same parameters described in the "Molecular dynamics search" section were used, except that the coordinates of the Mg^{2+} ion located at the active site (PDB file 2KTQ) were included. Na^+ and Cl^- ions were added to properly simulate the ion strength of the physiological solution and to neutralize the system. A snapshot taken every 25 ps was saved for further analysis. Additionally, three short runs of 10 ns each were performed starting from solution A, and three more starting from solution B, with different random number seeds being used to assign the initial velocities. When the seed number is changed, the chaotic nature of the molecular dynamics simulations ensures different trajectories, even when starting from the same conformations.

Results and discussion

Conformational space of 6,10,2′,6′-tetraacetyl-*O*-catalpol in solution

Based on a careful visual inspection, both methods of conformational search (see the "Methods" section) were

observed to yield similar results, indicating no biases relating to the conformational search method or the forcefield used. In order to quantify the preferential conformation in terms of the relative position of the terpenic fragment with respect to the glicosidic residue, we built a 2D Ramachandran-like conformational map from 24,000 conformations generated from two explicit solvent molecular dynamics trajectories, each lasting 300 ns, starting from different 6,10,2′,6′-tetraacetyl-*O*-catalpol conformations (see the "Molecular dynamics search" section). The mapped torsion angles α and β are defined as follows: α relates to C2′-C1′-$O_{anomeric}$-C1, while β relates to (C2′-C1′-$O_{anomeric}$-C9 (Fig. 2). As depicted in Fig. 2, there is one major highly populated basin that is centered at approximately $\alpha \approx \beta \approx 185°$. It is important to note that conformations outside this basin were also visited during the simulation, but these do not appear on the conformational map due to their low frequency of occurrence.

One snapshot was minimized, in vacuo, every nanosecond (600 conformations) using MOPAC 2009. The semi-empirical lowest energy conformation (Fig. 3) has torsion angles of α = 172.0° and β = 172.6° close to the basin found during the molecular dynamics study.

As we mentioned at the beginning of this section, The simulating annealing conformational search method yields similar results to the molecular dynamics search method (see the "Methods" section); on average, the torsion angles take values of $\alpha \approx 181°$ and $\beta \approx 176°$, and the low-energy conformation has α = 171.7° and β = 186.4°, indicating that there is no bias due to the conformational search method or forcefield used.

This highly restricted conformation space can be rationalized as the volume of the two rings plus the presence of the four acetyl groups.

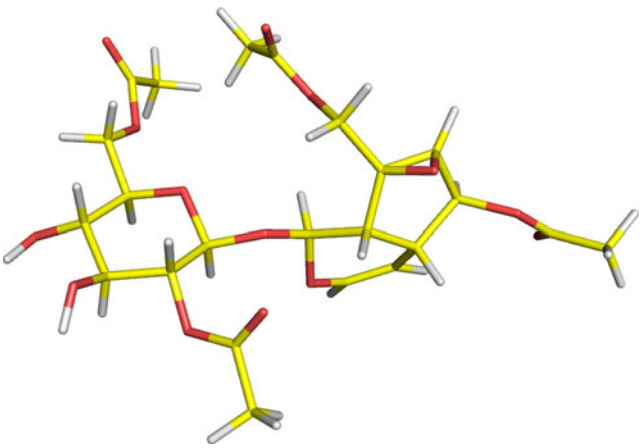

Fig. 3 The lowest energy conformation of 6,10,2′,6′-tetraacetyl-*O*-catalpol according to a classical molecular dynamics search followed by semi-empirical minimization. The torsion angles α = 172.0° and β = 172.6° are close to those of the basin found during the molecular dynamics study

Klentaq/DNA/6,10,2′,6′-tetraacetyl-*O*-catalpol docking complex

The Klentaq fragment, as well as other DNA polymerases, can adopt two states: the *open* and the *closed* states [22, 24]. In the latter, the dNTPs cannot enter the active site; in fact, the active site of the enzyme and the growing DNA helix are accommodated in such a manner that the incoming dNTP is tightly enclosed. Thus, in this work we analyzed the open state of the Klentaq fragment co-crystallized in the presence of a short DNA molecule and a ddCTP molecule, as resolved by X-ray diffraction (Protein Data Bank, identification code: 2KTQ).

Blind docking search

The molecular docking software Autodock 4.0 was used to explore the protein–DNA complex surface in the search for the most favorable binding site. This procedure is called blind docking, and Autodock has been shown to be able to perform this task [23]. The lowest energy cluster (the best energy solution of −4.45 kcal mol^{-1}) was located at the active site of the enzyme. This result is in line with our previous experimental observations regarding the inhibitory mechanism of catalpol [5], and supports the hypothesis of a competitive inhibitory mechanism for 6,10,2′,6′-tetraacetyl-*O*-catalpol. This blind docking step was followed by a more detailed docking procedure, as explained in the next section.

Focused docking search

In this section we describe the results of a ligand flexible docking search restricted to the binding site identified by Autodock, as described above. Among all of the docking solutions, we selected two clusters for further analysis. These corresponded to the two solutions with the lowest binding energies (−6.96 kcal mol^{-1} and −6.42 kcal mol^{-1}). At the same time, these clusters are the most highly populated (they have seven members each). According to Autodock, the inhibition constant (K_i) is estimated to be 7.85 μM and 19.55 μM for clusters 1 and 2, respectively. Both solutions locate 6,10,2′,6′-tetraacetyl-*O*-catalpol at a similar position to where the ddCTP is located in the file 2KTQ (Fig. 4) and thus, by extrapolation, to where the naturally occurring nucleotide to be added by the polymerase should be located. The torsion angles α and β of the first solution (A) pertain to the highly favorable basin found for 6,10,2′,6′-tetraacetyl-*O*-catalpol in solution, while α in the second solution (B) corresponds to an unfavorable value ($\alpha \approx 330°$). Also, solutions A and B differ in the position of 6,10,2′,6′-tetraacetyl-*O*-catalpol relative to the enzyme (Figs. 5 and 6). In the following section we describe a

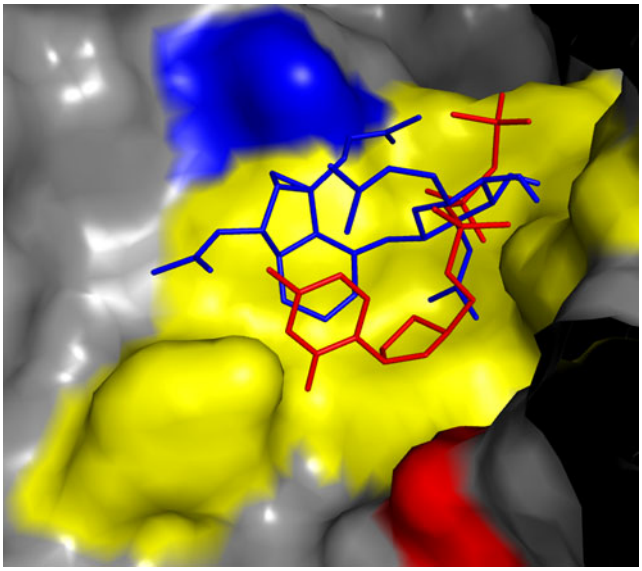

Fig. 4 The coordinates of 6,10,2′,6′-tetraacetyl-*O*-catalpol taken from the docked solution A and superimposed on the coordinates of the 2KTQ PDB file. 6,10,2′,6′-Tetraacetyl-*O*-catalpol (*blue*) and the ddCTP (*red*) occur at similar positions. The protein–DNA complex is shown as a *gray surface*, except for those protein residues that are neighbors of both 6,10,2′,6′-tetraacetyl-*O*-catalpol and ddCTP (residues D610, Y611, S612, Q613, I614, E615, K663, F667, L670, Y671, D785 and E786, in *yellow*), that are only neighbors of 6,10,2′,6′-tetraacetyl-*O*-catalpol (residue L616, in *blue*), or that are only neighbors of ddCTP (residue R573, in *red*). Neighbors are defined as any residues that have at least one atom that is closer than 4.5 Å to the corresponding ligand. The figures were created using Pymol [25]

series of molecular dynamics simulations that were performed to shed light on this issue.

Klentaq/DNA/6,10,2′,6′-tetraacetyl-*O*-catalpol molecular dynamics

In order to test the stabilities of the docked solutions, we submitted both to explicit solvent molecular dynamics. Two runs each lasting 30 ns were performed (see the "Methods" section).

Solution A

The superimposition of the docked solution on the trajectory-average conformation (Fig. 5) revealed that the terpenic fragment had moved 1.49 Å and the sugar fragment 1.73 Å from their initial positions. Part of this displacement is explained by a rotation along the main axis of the molecule, as depicted in Fig. 5. In the docked solution, the torsion angles were $\alpha \approx 183°$ and $\beta \approx 150,°$ and in the trajectory-average conformation $\alpha \approx 170°$ and $\beta \approx 192°$. Trajectory analysis indicated the presence of four hydrogen bonds between 6,10,2′,6′-tetraacetyl-*O*-catalpol and the enzyme that were present for >20% of the time (see Table 1). In summary, we observed that solution A was stable along the trajectory. 6,10,2′,6′-Tetraacetyl-*O*-catalpol fluctuated around its initial position relative to the protein–DNA complex, but this just seemed to be an adjustment inside the binding pocket, and it remained in almost the same conformation as its initial one near the in-solution basin.

Solution B

Visual inspection of the trajectory of solution B indicated that, before 1 ns was reached, the terpenic fragment and the 6′-acetyl moiety began to move away from the protein surface. Until ~7.5 ns, both the acetyl and the terpenic fragment were completely detached from the protein surface and outside the protein cavity in which they were originally located. This movement was followed by a change in the α torsion angle from values of around $\alpha \approx$

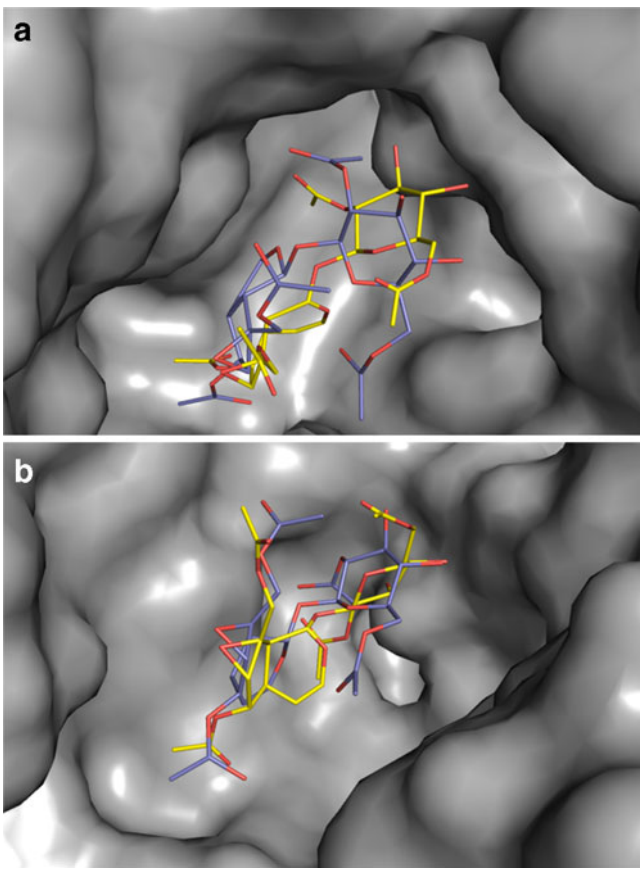

Fig. 5 **a**–**b** Docked solution A superimposed on the trajectory-averaged conformation of 6,10,2′,6′-tetraacetyl-*O*-catalpol starting from solution A. **a** Front view of the complex; the "palm" of the protein is facing the reader. **b** Top view of the protein; the DNA is under the 6,10,2′,6′-tetraacetyl-*O*-catalpol molecules. The protein–DNA complex is shown as a *gray surface*, the docked 6,10,2′,6′-tetraacetyl-*O*-catalpol is in *blue* (for carbons) and *red* (oxygens), the trajectory-averaged 6,10,2′,6′-tetraacetyl-*O*-catalpol is in *yellow* (for carbons) and *red* (oxygens), and hydrogens are not shown. The figures were created using Pymol [25]

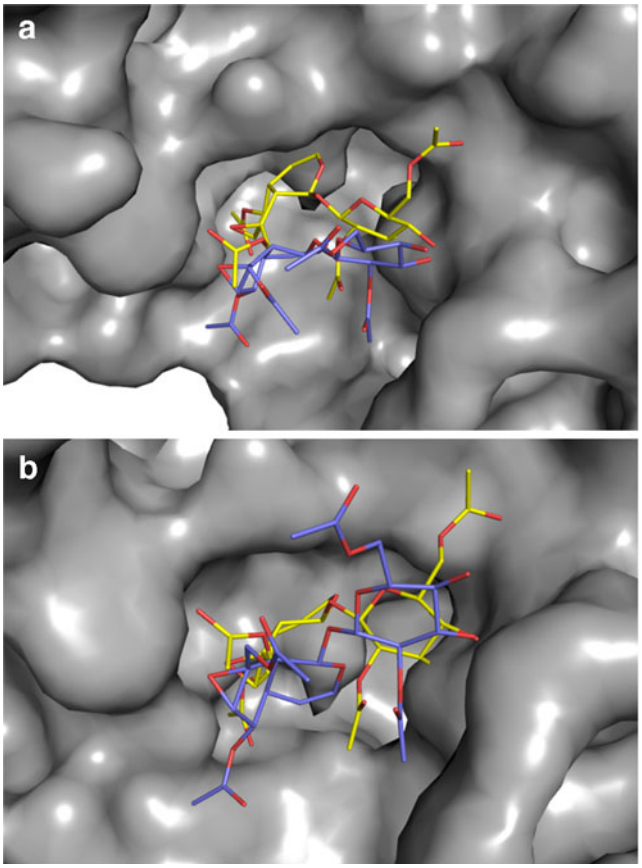

Fig. 6 **a**–**b** Docked solution B superimposed on the trajectory-averaged conformation of 6,10,2′,6′-tetraacetyl-*O*-catalpol starting from solution B. **a** Front view of the complex; the "palm" of the protein is facing the reader. **b** Top view of the protein; the DNA is under the 6,10,2′,6′-tetraacetyl-*O*-catalpol molecules. The protein–DNA complex is shown as a *gray surface*, the docked 6,10,2′,6′-tetraacetyl-*O*-catalpol is in *blue* (carbon) and *red* (oxygen), the trajectory-averaged 6,10,2′,6′-tetraacetyl-*O*-catalpol is in *yellow* (carbon) and *red* (oxygen), and hydrogens are not shown. The figures were created using Pymol [25]

340° to values of around $\alpha \approx 65°$. Comparison of the docked solution with the trajectory-averaged conformation (Fig. 6) shows that the terpenic fragment moves 4.1 Å and the sugar fragment 2.16 Å (this movement is mainly toward the solvent). Throughout most of the trajectory, the 6,10,2′,6′-tetraacetyl-*O*-catalpol (principally the terpenic fragment) is away from the binding pocket, and maintains contact with the protein mainly through two hydrogen bonds (3-OH and 4-OH act as donors to GLU 832 for 22.6% and 77.6% of the time, respectively). In brief, we can conclude that solution B was unstable along the trajectory. The 6,10,2′,6′-tetraacetyl-*O*-catalpol molecule moved away from its initial position toward the solvent (but it stayed near the active site), and it changed its conformation in terms of the α and β torsion angles (although it never visited the in-solution basin).

Moreover, six shorter molecular dynamics simulations were performed, each 10 ns long, to check the results of the 30 ns simulations. The three short-running simulations starting from solution A were stable and qualitatively in agreement with the corresponding long molecular dynamics. During the three short-running simulations starting from solution B, 6,10,2′,6′-tetraacetyl-*O*-catalpol detached from the surface of the enzyme. It seems that either the glycosidic or the terpenic fragment can initiate the detaching process. In summary, the molecular dynamics starting from solution A seemed to be more stable than those starting from solution B.

It is interesting to note that, from an entropic point of view, the rigidity of 6,10,2′,6′-tetraacetyl-*O*-catalpol in terms of the relative positions of the terpenic and glycosidic fragments favors solution A, because less conformational entropy is lost than in solution B; i.e., the bounded conformation of this derivate in solution A is almost the same as the unbounded conformation, in contrast to what was observed for solution B.

Conclusions

Blind docking indicates that the most favorable binding site is the active site of the enzyme, supporting the hypothesis of a competitive inhibition mechanism. This may be due to the molecular mimicry of iridoids and purine nucleosides (results that are comparable with those reported for catalpol [5]). A conformational ensemble of the complex protein/DNA/6,10,2′,6′-tetraacetyl-*O*-catalpol around solution A seems to be the most accurate proposal, although is not

Table 1 Hydrogen bonds detected during the molecular dynamics trajectory starting from solution A

Protein residue [a]	6,10,2′,6′-Tetraacetyl-*O*-catalpol atom	Hydrogen bond lifetime [b]
Arg 660 side chain	Carbonyl oxygen of 10-acetyl	20.39
Asp 610 side chain	4′-Hydroxyl	99.49
Tyr 611 backbone	3′-Hydroxyl	27.12
Thr 664 side chain	Epoxy oxygen	55.77

[a] Three-letter code for protein residue according to the numeration on the 2KTQ file

[b] Percentage of the snapshots in which a particular hydrogen bond was detected according to Yasara Dynamics

feasible to categorize solution B as being incorrect. Another valuable feature of the present work is that the simulations suggest further chemical modifications that can be made to 6,10,2′,6′-tetraacetyl-*O*-catalpol in order to increase its affinity to the KlenTaq fragment.

Acknowledgments Financial support from CONICET (PIP 00628), Universidad Nacional de San Luis (UNSL) (projects 22/Q805) (PROICO 328402) and Agencia Nacional para la Ciencia y Tecnología (ANPCyT) (PICT-2007-352) is gratefully acknowledged. O. A. Martin and H. A. Garro thank the Consejo Nacional de Investigaciones Científicas y Técnicas (CONICET) for their doctoral fellowships. C. R. Pungitore, M. Kurina Sanz, and C. E. Tonn are CONICET research staff. The research was conducted using an Intel quad-core I5-750 workstation and a Beowulf cluster at the Instituto de Matemática Aplicada San Luis (IMASL-CONICET). This work forms part of the Ph.D. thesis of Hugo A. Garro.

References

1. Newman DJ, Cragg GM, Snader KM (2003) Natural products as sources of new drugs over the period 1981–2002. J Nat Prod 66:1022–1037
2. El-Naggar LJ, Beal JL (1980) Iridoids: a review. J Nat Prod 43:649–707
3. Gotor V, Alfonso I, García-Urdiales E (2008) Asymmetric organic synthesis with enzymes. Weinheim, Wiley VCH
4. Bornscheuer UT, Kazlauskas RJ (2005) Hydrolases in organic synthesis, 2nd edn. Wiley-VCH, Weinheim
5. Pungitore CR, Ayub MJ, García M, Borkowski EJ, Sosa ME, Ciuffo G, Tonn CE (2004) Iridoids as allelochemicals and DNA polymerase inhibitors. J Nat Prod 67:357–361
6. Pungitore CR (2008) Natural products as inhibitors of DNA related enzymes: a review. Curr Enz Inhib 4:194–215
7. Pungitore CR, León LG, García C, Martín VS, Tonn CE, Padrón JM (2007) Novel antiproliferative analogs of the *Taq* DNA polymerase inhibitor catalpol. Bioorg Med Chem Lett 17:1332–1335
8. Garro HA (2008) Undergraduate thesis. Universidad Nacional de San Luis, San Luis
9. Allouche A (2010) What is Gabedit? http://gabedit.sourceforge.net/, accessed 21 June 2009
10. Stewart JJ (2010) MOPAC 2009. http://openmopac.net/, accessed 21 June 2009
11. Stewart JJ (2007) Optimization of parameters for semiempirical methods V: modification of NDDO approximations and application to 70 elements. J Mol Model 13:1173–1213
12. Van der Spoel D, Lindahl E, Hess B, Groenhof G, Mark AE, Berendsen HJ (2005) GROMACS: fast, flexible, and free. J Comput Chem 26:1701–1718
13. Hess B, Kutzner C, van der Spoel D, Lindahl E (2008) GROMACS 4: Algorithms for highly efficient, load-balanced, and scalable molecular simulation. J Chem Theor Comput 4:435–447
14. Schüttelkopf AW, van Aalten DM (2004) PRODRG: a tool for high-throughput crystallography of protein–ligand complexes. Acta Crystallogr D 60:1355–1363
15. Essmann U, Perera L, Berkowitz ML, Darden T, Lee H, Pedersen LG (1995) A smooth particle mesh Ewald method. J Chem Phys 103:8577–8593
16. Krieger E, Darden T, Nabuurs SB, Finkelstein A, Vriend G (2004) Making optimal use of empirical energy functions: force-field parameterization in crystal space. Proteins 57:678–683
17. Duan Y, Wu C, Chowdhury S, Lee MC, Xiong G, Zhang W (2003) A point-charge force field for molecular mechanics simulations of proteins based on condensed-phase quantum mechanical calculations. J Comput Chem 24:1999–2012
18. Vasilef I (2009) QtiPlot: data analysis and scientific visualization. http://soft.proindependent.com/qtiplot.html, accessed 21 June 2009
19. Morris GM, Goodsell DS, Halliday RS, Huey R, Hart WE, Belew RK (1998) Automated docking using a Lamarckian genetic algorithm and an empirical binding free energy function. J Comput Chem 19:1639–1662
20. Goodsell DS, Morris GM, Olson AJ (1996) Automated docking of flexible ligands: applications of AutoDock. J Mol Recognit 9:1–5
21. Berman HM (2000) The Protein Data Bank. Nucleic Acids Res 28:235–242
22. Li Y, Korolev S, Waksman G (1998) Crystal structures of open and closed forms of binary and ternary complexes of the large fragment of *Thermus aquaticus* DNA polymerase I: structural basis for nucleotide incorporation. EMBO J 17:7514–7525
23. Hetényi C, van Der Spoel D (2002) Efficient docking of peptides to proteins without prior knowledge of the binding site. Protein Sci 11:1729–1737
24. Golosov AA, Warren JJ, Beese LS, Karplus M (2010) The mechanism of the translocation step in DNA replication by DNA polymerase I: a computer simulation analysis. Structure 18:83–93
25. Schrödinger L (2010) The PyMOL molecular graphics system, v.1.2r1. http://www.pymol.org/, accessed 21 June 2009